Weierstraß-Institut

für Angewandte Analysis und Stochastik

im Forschungsverbund Berlin e. V.

Preprint ISSN 0946 – 8633

A Numerical Method for Mass Conservative Coupling Between Fluid Flow and Solute Transport

Jürgen Fuhrmann[12], Hartmut Langmach[13], Alexander Linke[14]

submitted: 15 June 2010

[1] Weierstrass Institute for Applied Analysis and Stochastics,
Mohrenstr. 39, 10117 Berlin, Germany

[2] Email: juergen.fuhrmann@wias-berlin.de [3] Email: hartmut.langmach@wias-berlin.de

[4] Email: alexander.linke@wias-berlin.de

No. 1521

Berlin 2010

2010 *Mathematics Subject Classification.* 76V05 76D05 65N08 65N30.

2008 *Physics and Astronomy Classification Scheme.* 47.10.ad 47.11.Fg 47.11.Hj 82.20.Wt.

Key words and phrases. Incompressible Navier-Stokes Equations, Convection-Diffusion Equation, Finite Element Method, Finite Volume Method, Electrochemical Flow Cell, Limiting Current.

Edited by
Weierstraß-Institut für Angewandte Analysis und Stochastik (WIAS)
Mohrenstraße 39
10117 Berlin
Germany

Fax: +49 30 2044975
E-Mail: preprint@wias-berlin.de
World Wide Web: http://www.wias-berlin.de/

Abstract

We present a new coupled discretization approach for species transport in an incompressible fluid. The Navier-Stokes equations for the flow are discretized by the divergence-free Scott-Vogelius element on barycentrically refined meshes guaranteeing LBB stability. The convection-diffusion equation for species transport is discretized by the Voronoi finite volume method. In accordance to the continuous setting, due to the exact integration of the normal component of the flow through the Voronoi surfaces, the species concentration fulfills discrete global and local maximum principles. Besides of the the numerical scheme itself, we present important aspects of its implementation. Further, for the case of homogeneous Dirichlet boundary conditions, we give a convergence proof for the coupled scheme. We report results of the application of the scheme to the interpretation of limiting current measurements in an electrochemical flow cell with cylindrical shape.

1 Introduction

We describe an algorithm which uses the Voronoi box based finite volume method in order to calculate solute transport in a given flow field $\vec{v}$. In the case of an incompressible, dilute solution, local mass conservation and maximum principles for this problem are directly connected to the condition $\nabla \cdot \vec{v} = 0$. If the flow field is given as the result of a numerical computation, a discrete analogon of that condition is required in order to guarantee mass conservation. A possible resort for this problem is the Scott-Vogelius element P_k-P_{k-1}^{disc} with polynomial order $k \geq 1$ which guarantees a pointwise divergence-free discrete flow field. This mixed finite element is LBB stable on regular, barycentrically refined simplicial meshes with a polynomial order of $k \geq d$, d the space dimension[30, 20]. Different aspects of this discretization method for the incompressible Navier-Stokes equations have been studied in more detail in [18, 4]. In this paper we present a numerical scheme which couples the Scott-Vogelius element for the incompressible flow problem and the Voronoi finite volume method for the species concentrations in a straightforward manner by using exact integration of the normal component of the discrete flow through the faces of the Voronoi control volumes.

In [19] different strategies are proposed in order to obtain a mass conservative coupling between Navier-Stokes flow and solute transport using finite element methods for both problems. Additional conditions on the Navier-Stokes discretization are necessary in order to obtain mass conservation in discretized convection-diffusion equations. With these strategies, at least global mass conservation can be achieved, but features of the original continuous problem like maximum principles and positivity are not preserved. The failure of discrete maximum principles is typical for stabilized finite element

methods for convection-diffusion equations [14, 15], but occurs in general also for pointwise divergence-free flow fields. On the other hand, on boundary conforming Delaunay meshes, upwinded Voronoi finite volume methods always fulfill these qualitative properties [26, 11].

In [5] a similar coupling approach is studied. The authors present a scheme for density driven flow based on a Taylor-Hood finite element method for the flow and on a Donald box based finite volume method for the hyperbolic transport equation. Coupling is performed by postprocessing the finite element velocity by defining an auxiliary discretely divergence-free velocity for use in the finite volume scheme. They consider instationary problems and take special care of the influence of the density variations on the flow. They verify their method by different numerical experiments.

In section 2, we present the weak formulation of the problem. Section 3 is devoted to the description of the discretization scheme. Based on compactness arguments, we give a convergence proof for the coupled scheme in the case of Dirichlet boundary conditions. In section 4, we discuss a method to calculate boundary fluxes based on volume integration and we discuss maximum principles for the transport equation. In section 5, we elaborate on several implementation issues. In section 6, we apply the presented method to the interpretation of a limiting current experiment in an electrochemical flow cell [12]. In particular, we demonstrate the consequences of the violation of the discrete divergence condition when using the same coupling approach with the Taylor-Hood element.

2 Problem formulation

Let $\Omega \subset \mathbb{R}^d$ be a simply connected Lipschitz domain with $d \in \{2,3\}$. We regard the stationary, incompressible Navier-Stokes equations coupled to the equation of stationary transport of a dissolved species under the assumption that the solution is dilute which allows to ignore the influence of density variations on the fluid flow. Therefore, the flow is described using the steady, incompressible Navier-Stokes equations:

$$(\vec{v}\cdot\nabla)\vec{v} + \nabla p - \eta\Delta\vec{v} = \vec{f}, \qquad \nabla\cdot\vec{v} = 0. \tag{2.1}$$

Here, $\vec{v}$ is the fluid velocity, p is the pressure, η is the viscosity of the fluid, and $\vec{f}$ is a force vector. The steady transport of a species dissolved in the fluid is described by the system

$$\nabla\cdot\vec{q} = s, \quad \vec{q} = -(D\nabla c - c\vec{v}) \tag{2.2}$$

Here, $\vec{q}$ is the species molar flux, c is the species molar concentration, D is the diffusion coefficient, $\vec{v}$ is the fluid velocity which is a solution of (2.1), and s is a given source term.

The boundary conditions correspond to a physical problem under investigation – the limiting current problem in a flow cell [13, 12]. For a thorough description of this background, we refer to section 6. Let $\mathscr{I}_\Gamma = \{A, I, O, S, W\}$ be a set of labels for boundary

sections. We assume that the boundary $\Gamma = \partial\Omega = \bigcup_{i\in\mathscr{I}_\Gamma}\Gamma_i$ is subdivided into an inlet Γ_I, an outlet Γ_O, an anode Γ_A, and a symmetry boundary on Γ_S. The remaining part of Γ is assumed to consist of inert, impermeable walls Γ_W. We further assume that $\Gamma_A, \Gamma_I, \Gamma_O$ are separated from each other by sections belonging either to Γ_W or Γ_S. We impose the following boundary conditions:

Section	c	$(\vec{v}, p)$
Inlet Γ_I	$c = c_I(x)$	$\vec{v} = \vec{v}_I(\vec{x})$
Anode Γ_A	$c = 0$	$\vec{v} = \vec{0}$
Outlet Γ_O	$\frac{\partial c}{\partial \vec{n}} = 0$	$\eta \frac{\partial \vec{v}}{\partial \vec{n}} = p\vec{n}$
Symmetry Γ_S	$\frac{\partial c}{\partial \vec{n}} = 0$	$\vec{v}\cdot\vec{n} = 0,\ \frac{\partial(\vec{v}\cdot\vec{t})}{\partial \vec{n}} = 0$
Wall Γ_W	$\frac{\partial c}{\partial \vec{n}} = 0$	$\vec{v} = \vec{0}$.

(2.3)

Let $\Gamma_D^{\mathrm{NS}} = \Gamma_I \cup \Gamma_A \cup \Gamma_W$ denote the Dirichlet boundary for the Navier-Stokes equations and let

$$V = \{\vec{v} \in [H^1(\Omega)]^d | \vec{v} = \vec{v}_D \,\mathrm{on}\, \Gamma_D^{\mathrm{NS}}, \vec{v}\cdot\vec{n} = 0 \,\mathrm{on}\, \Gamma_S\},$$

where v_D is defined by corresponding boundary values in (2.3). We derive a new right hand side $\vec{f}$ from the extension of $\vec{v}_D$ into Ω and then assume that the solution $\vec{v}$ is in V, thus removing all integrals over Γ_D.

After multiplication of (2.1) with a sufficiently smooth test function $(\vec{w}, q)$, all boundary integrals cancel out, and the weak formulation of (2.1) is given as follows: Find $(\vec{v}, p) \in V \times L^2(\Omega)$ such that for all $(\vec{w}, q) \in V \times L^2(\Omega)$

$$\int_\Omega \eta \nabla\vec{v} : \nabla\vec{w}\, dx + \int_\Omega ((\vec{v}\cdot\nabla)\vec{v})\cdot\vec{w}\, dx + \int_\Omega p\nabla\cdot\vec{w}\, dx = \int_\Omega \vec{f}\cdot\vec{w}\, dx; \qquad \int_\Omega q\nabla\cdot\vec{v}\, dx = 0. \tag{2.4}$$

The weak formulation of (2.2) relies on the particular choice of boundary conditions for $\vec{v}$. Let $\Gamma_D^T = \Gamma_A \cup \Gamma_I$ be the Dirichlet boundary for the transport equation, and let s be the right hand side containing the Dirichlet boundary conditions. Let $W = \{c \in H^1(\Omega) |\, c|_{\Gamma_D^T} = 0\}$. Then we look for $c \in W$ such that for all $\phi \in W$,

$$\int_\Omega (D\nabla c - c\vec{v})\cdot\nabla\phi\, dx + \int_{\Gamma_O} \vec{v}\cdot\vec{n} c\phi\, ds = \int_\Omega s\phi\, dx. \tag{2.5}$$

The existence of the solution of (2.5) can be proven by the Lax-Milgram lemma. For coercivity, it is essential that $\vec{v}\cdot\vec{n} \geq 0$ a.e. on Γ_O which we can expect if we assume that $\vec{v}\cdot\vec{n} \leq 0$ a.e. on Γ_I.

The system (2.4), (2.5) can be analyzed and solved in a decoupled manner. The first step is the treatment of (2.4) yielding a steady velocity field $\vec{v}$. In a second step using this velocity field, we treat (2.5) resulting in a steady solute distribution c. The convergence analysis in section 3 in this paper will be delivered for the "all Dirichlet" case $\Gamma_I = \Gamma$ which we then can assume as a special case of the boundary conditions (2.3).

For the flow cell example in section 6, we will assume $c_I(\vec{x}) = \hat{c}_I$ to be constant, and $\vec{v}_I(\vec{x})$ to be derived from a Hagen Poiseuille like profile, and that the source terms $\vec{f}, s$ in (2.1), (2.2) are zero.

3 Coupled finite volume and finite element discretization

The coupled discretization scheme is based on two independent discretization meshes, one for the Navier-Stokes equations, and another one for the transport equation. The coupling is achieved by the calculation of the normal projection of the velocity from the finite element scheme onto the facets of the control volumes. In the sequel, we give an independent description of both schemes.

3.1 Finite element discretization

We introduce two different conforming Galerkin mixed finite element discretizations for the incompressible Navier-Stokes equations. They are derived directly from the weak formulation in (2.4) by choosing finite-dimensional function spaces $V_h \subset V$ and $P_h \subset L^2(\Omega)$ which serve as trial and test function spaces. The main focus of the paper will be on the Scott-Vogelius mixed finite element, which delivers pointwise divergence-free, discrete velocity approximations. The convergence proof of the coupling scheme is elaborated for the Scott-Vogelius element, With small changes, it could also be extended to the Taylor-Hood element.

Let $\bar{\mathscr{T}}_h$ denote a regular finite element triangulation of the domain Ω in the sense of [6]. The mesh $\bar{\mathscr{T}}_h$ is called a macro triangulation and we derive a second triangulation $\mathscr{T}_h$ from $\bar{\mathscr{T}}_h$. For each simplex $\bar{T} \in \bar{\mathscr{T}}_h$ we connect its barycenter with its vertices, and we thereby get three new triangles from each macro triangle, or four new tetrahedra from each macro tetrahedron. This new triangulation $\mathscr{T}_h$ is also locally shape regular and locally quasi-uniform, although the constants for interpolation estimates are worse, because we get larger angles. In the following, such a shape-regular and barycentrically refined mesh will be called an admissible mesh for the Scott-Vogelius element.

For the Taylor-Hood element and the Scott-Vogelius element in space dimension d, we define V_h as the space of continuous elementwise vector functions of polynomial order $d+1$ on the triangulation $\mathscr{T}_h$

$$V_h := \left\{ \vec{v}_h \in [C(\Omega)]^d \cap V : \vec{v}_{h|T} \in [P_{d+1}(T)]^d, \text{for all } T \in \mathscr{T}_h \right\}.$$

Though these two mixed finite elements have the same discrete velocity space, they differ in the discrete pressure space. For the Taylor-Hood element we define

$$P_h^{\mathrm{TH}} := \left\{ q \in L^2(\Omega) \cap C(\Omega) : q_{|T} \in P_{d-1}, \text{for all } T \in \mathscr{T}_h \right\},$$

while the pressure space of the Scott-Vogelius element is defined by

$$P_h^{\mathrm{SV}} := \left\{ q \in L^2(\Omega) : q_{|T} \in P_{d-1}, \text{for all } T \in \mathscr{T}_h \right\}.$$

Therefore the Taylor-Hood element and the Scott-Vogelius element have elementwise linear pressure functions in two dimensions and elementwise quadratic pressure functions in three dimensions, but for the latter the pressure functions are discontinuous.

The above derivation of the triangulation $\mathscr{T}_h$ from a macro-triangulation $\tilde{\mathscr{T}}_h$ assures that the Scott-Vogelius element is LBB stable on $\mathscr{T}_h$ [20, 2, 30]. Also the LBB stability of the Taylor-Hood element is assured on such triangulations [3].

The discretization of the problem in equation (2.4) is now given as follows: find $(\vec{v}_h, p_h) \in V_h \times P_h$ with $P_h \in \{P_h^{\mathrm{TH}}, P_h^{\mathrm{SV}}\}$ such that

$$\begin{aligned}\int_\Omega (\vec{v}_h \cdot \nabla)\vec{v}_h \cdot \vec{w}_h \, dx - \int_\Omega p_h \nabla \cdot \vec{w}_h \, dx + \int_\Omega \eta \nabla \vec{v}_h : \nabla \vec{w}_h \, dx = \int_\Omega \vec{f} \cdot \vec{w}_h \, dx \\ - \int_\Omega q_h \nabla \cdot \vec{v}_h \, dx = 0,\end{aligned} \tag{3.1}$$

which holds for all test functions $(\vec{w}_h, q_h) \in V_h \times P_h$.

The Scott-Vogelius element is interesting for our investigation below, since its discrete velocity space and its discrete pressure space fulfill an important property, namely

$$\nabla \cdot V_h \subset P_h^{\mathrm{SV}}. \tag{3.2}$$

This property enforces exact mass conservation of the Scott-Vogelius element in the L^2 sense, since we can choose the special test function $q_h := -\nabla \cdot \vec{v}_h$ in equation (3.1)

$$0 = -\int_\Omega q_h \nabla \cdot \vec{v}_h \, dx = \int_\Omega (\nabla \cdot \vec{v}_h)^2 \, dx.$$

In general, the same pressure test function cannot be used in the Taylor-Hood case, since $\nabla \cdot V_h \not\subset P_h^{\mathrm{TH}}$. Hence the Taylor-Hood element only delivers discretely divergence-free approximations $\vec{v}_h$, and this will arise below as the proper origin of violations in the discrete maximum principle for a coupled transport equation.

3.2 Voronoi Finite Volumes on boundary conforming Delaunay meshes for solute transport

In order to describe the finite volume scheme, we first introduce some notations. Assume that $\partial\Omega$ is the union of planar polygons. Let $\mathscr{P} = \{\vec{x}_K\} \subset \bar{\Omega}$ a set of points which includes all the vertices of the polygons constituting $\partial\Omega$. A simplicialization of this point set has the Delaunay property if no circumball of any simplex contains a point $\vec{x}_K$ of $\mathscr{P}$. For a given point $\vec{x}_K \in \mathscr{P}$, the Voronoi cell $V_K^0 \subset \mathbb{R}^d$ around $\vec{x}_K$ is defined as the set of points $\vec{x} \in \mathbb{R}^d$ which are closer to $\vec{x}_K$ than to any other point $\vec{x}_L$ of $\mathscr{P}$. The set of Voronoi cells is called Voronoi diagram. The duality of the Voronoi diagram and the Delaunay simplicialization allows to calculate the Voronoi cell around $\vec{x}_K$ by joining the circumcenters of the simplices having $\vec{x}_K$ in common.

We define as the control volume around $\vec{x}_K$ the Voronoi box V_K associated with $\vec{x}_K$ as $V_K = V_K^0 \cap \Omega$. For a proper construction, the simplicialization of the point set in addition to the Delaunay property has to be boundary conforming [26]. In the present context this means that

1 Ω is the union of all simplices;

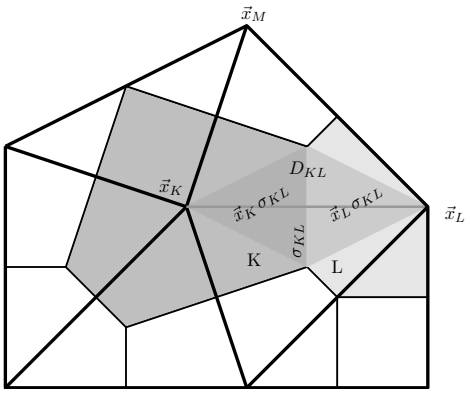

Figure 1: A control volume K around the node of the simplicial mesh $\vec{x}_K$, the Voronoi box face σ_{KL} and the diamond set D_{KL} coresponding to two neigboring control volumes K, L.

2 no simplex circumball contains any other discretization vertex;

3 all simplex circumcenters are contained in $\bar{\Omega}$;

4 the boundary sections Γ_i ($i \in \mathscr{I}_\Gamma$) are the unions of simplex faces, and all circumcenters of boundary simplices from Γ_i are contained in $\bar{\Gamma}_i$.

In this situation, it is possible to explicitely construct the boundaries ∂V_K of the Voronoi boxes, see section 5.1.1.

The set of Voronoi boxes generates an admissible finite volume partition in the sense of [8] (where in the latter, one needs to replace "edge" by "face"). In order to simplify notations and to get them synchronized with [8], in the sequel, we will use K in order to denote the the Voronoi boxes V_K.

Let $\mathscr{K}$ denote the set of control volumes K, and $\mathscr{K}_i$ denote the set of control volumes K which share facets with Γ_i. Let $\mathscr{K}_D = (\mathscr{K}_I \cup \mathscr{K}_A)$ denote the set of Dirichlet control volumes and $\mathscr{K}^0 = \mathscr{K} \setminus \mathscr{K}_D$ denote the set of non-Dirichlet control volumes. We assume that the set of control volumes is ordered linearly by a relation $\prec$.

For two control volumes K, L, let $\sigma_{KL} = \partial K \cap \partial L$. If $|\sigma_{KL}| > 0$, then K, L are called neighbours and $\vec{x}_K\vec{x}_L$ is an edge of the boundary conforming Delaunay simplicialization which is known to be orthogonal to σ_{KL}. Let $D_{KL} = \vec{x}_K\sigma_{KL} \cup \vec{x}_L\sigma_{KL}$ denote the union of the pyramides spanned by σ_{KL} and $\vec{x}_K, \vec{x}_L$, respectively, also called diamond. Let $\mathscr{E} = \{K|L \mid K \prec L \text{ and } |\partial K \cap \partial L| > 0\}$ denote the set of all pairs of neighbouring control volumes. Let $\mathscr{N}_K = \{L \in \mathscr{K} \mid K|L \in \mathscr{E}\}$ denote the set of neighbours of K. For $i \in \mathscr{I}_\Gamma$, let $\mathscr{G}_K^i$ be the set of facets of K with nonempty intersection with the boundary part Γ_i. Then $\partial K \cap \Gamma_i = \bigcup_{\sigma \in \mathscr{G}_K^i} \sigma$ and

$$\partial K = \left(\bigcup_{K|L \in \mathscr{N}_K} \sigma_{KL} \right) \cup \left(\bigcup_{i \in \mathscr{I}_\Gamma} (\cup_{\sigma \in \mathscr{G}_K^i} \sigma) \right).$$

Let $\partial\mathscr{E} = \bigcup_{K\in\mathscr{K},i\in\mathscr{I}_\Gamma} \mathscr{G}_K^i$ denote the set of boundary facets, and $\bar{\mathscr{E}} = \mathscr{E}\cup\partial\mathscr{E}$. For the definition of the regularity of a finite volume discretization we refer to [8].

For any facet $\sigma\in\bar{\mathscr{E}}$ we define the scaled normal

$$\vec{h}_\sigma = \begin{cases} \vec{h}_{KL} = \vec{x}_L - \vec{x}_K, & \sigma = \sigma_{KL}, K|L \in \mathscr{E} \\ \vec{n}_\Omega^{out}, & \sigma\in\partial\mathscr{E} \end{cases}$$

and the transmission coefficients

$$\tau_\sigma = \begin{cases} \tau_{KL} = \frac{|\sigma_{KL}|}{|\vec{h}_{KL}|} & \sigma = \sigma_{KL}, K|L\in\mathscr{E} \\ |\sigma|, & \sigma\in\partial\mathscr{E}. \end{cases}$$

Let $h_\sigma = |\vec{h}_\sigma|$.

Obviously, $\Omega = \bigcup_{K|L\in\mathscr{E}} D_{KL}$, therefore

$$d|\Omega| = d\sum_{K|L\in\mathscr{E}} |D_{KL}| = d\sum_{K|L\in\mathscr{E}} |D_{KL}| = d\sum_{K|L\in\mathscr{E}} \frac{|\sigma_{KL}|h_{KL}}{d} = \sum_{K|L\in\mathscr{E}} |\sigma_{KL}|h_{KL} \tag{3.3}$$

Let $\vec{v}\in[H^1(\Omega)]^d$ fulfill the boundary conditions (2.3) and $\nabla\cdot\vec{v} = 0$. We note that every solution $\vec{v}$ of (2.4) and every Scott-Vogelius solution $\vec{v}_h$ of (3.1) fulfills this criterion. For any $\sigma\in\bar{\mathscr{E}}$, the H^1-regularity of $\vec{v}$ allows to define the scaled flux projection

$$v_\sigma = \frac{1}{|\sigma|}\int_\sigma \vec{v}\cdot\vec{h}_\sigma ds. \tag{3.4}$$

These flux projections are discretely divergence-free in the sense that for all $K\in\mathscr{K}$ holds

$$\sum_{L\in\mathscr{N}_K} \tau_{KL} v_{\sigma_{KL}} + \sum_{i\in\mathscr{I}}\sum_{\sigma\in\mathscr{G}_K^i} \tau_\sigma v_\sigma = 0. \tag{3.5}$$

We introduce the space of functions

$$W_h = \{c_h\in L^2(\Omega)\colon c_{h|K} = c_K\},$$

consisting of scalar functions which are piecewise constant on each control volume. Here, $c_K = c_{h|K}$ is an approximation of $c(\vec{x}_K)$ in the control volume K, see [8]. Further, we define the discrete right-hand side of the discrete convection-diffusion equation by the average value of the continuous right-hand side over the control volume K

$$s_K = \frac{1}{|K|}\int_L s(\vec{x})\,dx.$$

Then, the finite volume scheme for the transport equation (2.5) reads as: we look for $c_h\in W_h$ such that

$$\begin{cases} \sum_{L\in\mathscr{N}_K} \tau_{KL} g(c_K, c_L, v_{\sigma_{KL}}) + \sum_{\sigma\in\mathscr{G}_K^O} \tau_\sigma g(c_K, c_K, v_\sigma) = s_K & K\in\mathscr{K}^0 \\ c_K = c_D(\vec{x}_K), & K\in\mathscr{K}_D, \end{cases} \tag{3.6}$$

where the treatment of the outflow boundary conditions is taken from [11].

The scheme is motivated by an approximation of

$$\int_K \nabla \cdot \vec{q}\, dx = \sum_{L \in \mathcal{N}_K} \tau_{KL} \frac{1}{|\sigma|} \int_{\sigma_{K|L}} \vec{q} \cdot \vec{h}_{\sigma_{KL}}\, ds + \sum_{\sigma \in \mathcal{G}_K} \tau_\sigma \int_\sigma \vec{q} \cdot \vec{h}_\sigma ds$$

i.e., the flux function $g(c_K, c_L, v_{\sigma_{KL}})$ is an approximation of the average normal flux

$$\frac{1}{|\sigma_{KL}|} \int_{\sigma_{KL}} \vec{q} \cdot \vec{h}_{\sigma_{KL}} ds$$

through the facet σ_{KL} scaled by $h_{\sigma_{KL}}$. Like in [11], for a given function $U(z)$, we set

$$g(c_K, c_L, v) = D\left(U\Big(\frac{v}{D}\Big)\, c_K - U\Big(-\frac{v}{D}\Big)\, c_L\right), \tag{3.7}$$

For $U(z) = U_{\mathrm{dcd}}(z) = 1 + \frac{z}{2}$ we yield the sum of the standard finite difference for the diffusion part and the central difference scheme. As $U_{\mathrm{dcd}}(z) < 0$ for $z < -2$, the such generated numerical flux g does not fulfill the monotonicity conditions necessary for stability [11]. Therefore, we demand that he function $U(z)$ is positive for all $z \in \mathbb{R}$. The simple upwind discretization is given by the upwind function

$$U_{\mathrm{dsu}}(z) = \begin{cases} 1+z & z \geq 0 \\ 1 & z < 0 \end{cases}.$$

A preferable choice for the function U going back to Allen and Southwell [1] is the Bernoulli function

$$U_{\exp}(z) = B(z) = \frac{z}{1 - e^{-z}}. \tag{3.8}$$

leading to the the so-called exponential fitting scheme which delivers exact flux approximations for linear, one-dimensional convection-diffusion equations with constant coefficients and a constant right hand side.

In the following, we will use the even and the odd part of a given function $U(z)$ which is defined by

$$U_{\mathrm{even}}(z) := \frac{1}{2}\left(U(z) + U(-z)\right), \qquad U_{\mathrm{odd}}(z) := \frac{1}{2}\left(U(z) - U(-z)\right).$$

We have by definition $U(z) = U_{\mathrm{even}}(z) + U_{\mathrm{odd}}(z)$. For all the three functions $U_{\mathrm{odd}}(z)$ above, we obtain

$$U_{\mathrm{odd}}(z) = \frac{z}{2}. \tag{3.9}$$

Therefore, the flux between two control volumes K and L is only convective, when $c_K = c_L$, i.e.,

$$g(c_K, c_K, v) = D\left(U\Big(\frac{v}{D}\Big)\, c_K - U\Big(-\frac{v}{D}\Big)\, c_K\right) = 2DU_{\mathrm{odd}}\Big(\frac{v}{D}\Big)\, c_K = c_K v.$$

This fact motivates the treatment of the outflow boundary.

The even parts are given by

$$
\begin{aligned}
U_{\mathrm{dcd,even}}(z) &= 1, \\
U_{\mathrm{dsu,even}}(z) &= 1 + \frac{|z|}{2}, \\
U_{\mathrm{exp,even}}(z) &= \frac{z}{2}\coth\left(\frac{z}{2}\right) = 1 + \mathscr{O}(z^2).
\end{aligned}
$$

Altogether, for all three functions $U_{\mathrm{even}}(z)$ we have the important relations

$$
1 \leq U_{\mathrm{even}}(z) \leq 1 + \frac{|z|}{2} \quad \text{and} \quad \lim_{z\to 0} U_{\mathrm{even}}(z) = 1. \tag{3.10}
$$

With these functions we can write (3.7) as

$$
g(c_K, c_L, v) = DU_{\mathrm{even}}\left(\frac{v}{D}\right)(c_K - c_L) + \frac{c_K + c_L}{2}v. \tag{3.11}
$$

The convergence proof below relies mainly on the relations (3.9) and (3.10). It is imaginable, of course, to use other approximations $U(z)$ for the flux with similar properties.

3.3 Convergence of the coupled FVM-FEM scheme

In the following we deliver a convergence analysis for the coupled scheme with the Scott-Vogelius element for the fluid flow discretization, and the Voronoi finite volume method for the transport equation. Our proof is based on compactness arguments.

In order to limit the complexity of the convergence analysis, we introduce homogeneous Dirichlet boundary conditions on $\Gamma = \partial\Omega$:

$$
c|_\Gamma = 0 \quad \vec{v}|_\Gamma = \vec{0} \tag{3.12}
$$

Generalization to inhomogeneous Dirichlet boundary conditions is straightforward using the standard technique of subtracting an extension of the boundary value to the domain, and thus moving the treatment of the inhomogeneous boundary conditions to the right hand sides $\vec{f}$, s. As a consequence, in the weak formulations (2.4) and (2.5), we assume that $\Gamma = \Gamma_I$ with the consequence that $\vec{v} \in V = [H_0^1(\Omega)]^d$ and $c \in H_0^1(\Omega)$.

For the proof of the coupled scheme, we investigate a sequence of mesh pairs $(\mathscr{T}_h, \mathscr{V}_h)$ which is indexed by the mesh parameter h. $\mathscr{T}_h$ denotes a sequence of regular, barycentric refined simplicial meshes in the sense above, $\mathscr{V}_h$ denotes a sequence of regular Voronoi meshes. The only geometrical assumption which relates both sequences of meshes is that their respective mesh parameters $h_{\mathrm{FEM}}(h)$ and $h_{\mathrm{FVM}}(h)$ go uniformly to zero, i.e., there are constants C_1 and C_2 which are independent of h and the relation

$$
C_1 h_{\mathrm{FEM}}(h) \leq h_{\mathrm{FVM}}(h) \leq C_2 h_{\mathrm{FEM}}(h)
$$

holds. We further assume that both mesh sequences possess uniform bounds for their mesh regularities.

3.3.1 Convergence of the Scott-Vogelius finite element method

Lemma 3.1. *The Scott-Vogelius discretization* (3.1) *has at least one discrete solution* $(\vec{v}_h, p_h)$ *on every grid, which is admissible in the sense above.*

Proof. This is a classical result, see e.g. [28]. In order to obtain the result, we introduce the subspace of divergence-free functions for the Scott-Vogelius finite element method

$$V_{0,h} = \{\vec{v}_h \in V_h \colon \nabla \cdot \vec{v}_h = 0\} \tag{3.13}$$

and we reformulate the above weak problem (3.1) as a problem without the pressure p_h: we look for $\vec{v}_h \in V_{0,h}$ such that

$$\int_\Omega \eta \nabla \vec{v}_h : \nabla \vec{w}_h \, dx + \int_\Omega (\vec{v}_h \cdot \nabla) \vec{v}_h \cdot \vec{w}_h \, dx = \int_\Omega \vec{f} \cdot \vec{w}_h \, dx \tag{3.14}$$

holds for all $\vec{w}_h \in V_{0,h}$. Then, we apply Brouwer's fixed point theorem, see [28], and obtain at least one solution $\vec{v}_h \in V_{0,h}$ such that (3.14) holds. Then, for each solution $\vec{v}_h \in V_{0,h}$ there is a unique, corresponding discrete pressure p_h which exists due to the discrete LBB stability of the Scott-Vogelius element on admissible meshes. □

In the following, we are only interested in discrete velocity solutions of the steady Navier-Stokes problem in (3.14) without the pressure, since the pressure does not occur in the coupling procedure.

Lemma 3.2. *For a sequence of Scott-Vogelius solutions* $(\vec{v}_h)$ *in* (3.14) *we can extract a subsequence which converges weakly in* $V = [H_0^1(\Omega)]^d$ *to some* $\vec{v} \in V$*. Moreover, this convergence is strong in* $[L^2(\Omega)]^d$ *and the limit* $\vec{v}$ *is divergence-free.*

Proof. Testing with $\vec{w}_h = \vec{v}_h$ in (3.14) and using the Poincaré inequality yields

$$\|\nabla \vec{v}_h\|_0 \leq \frac{C_F}{\eta} \left\| \vec{f} \right\|_0$$

with the Poincaré constant C_F. By Rellich's theorem we obtain that a subsequence of $(\vec{v}_h)$ converges weakly in $[H_0^1(\Omega)]^d$ to some $\vec{v} \in V$. This subsequence is denoted again as $(\vec{v}_h)$. Moreover, we know by Rellich's theorem that the sequence converges strongly in $[L^2(\Omega)]^d$ to $\vec{v}$. For any regular test function $\psi \in C_0^\infty(\Omega)$ it holds further

$$\int_\Omega \vec{v} \cdot \nabla \psi \, dx = \lim_{h \to 0} \int_\Omega \vec{v}_h \cdot \nabla \psi \, dx = 0.$$

Therefore, the limit $\vec{v}$ is divergence-free. □

Theorem 3.1. *The limit* $\vec{v}$ *of the sequence of Scott-Vogelius solutions* $(\vec{v}_h)_h$ *from Lemma 3.2 is a solution of the steady Navier-Stokes problem* (2.4)*, and we obtain*

$$\vec{v}_h \overset{H_0^1}{\to} \vec{v}.$$

Proof. Since we know from Lemma 3.2 that $\vec{v}$ is divergence-free, we have to prove only that $\vec{v}$ fulfills the momentum equation of (2.4). For that we choose an arbitrary, divergence-free velocity test function $\vec{\varphi} \in [C_0^\infty(\Omega)]^d$ and we must check that $\vec{v}$ fulfills

$$\int_\Omega (\vec{v}\cdot\nabla)\vec{v}\cdot\vec{\varphi}\,dx + \int_\Omega \eta\nabla\vec{v} : \nabla\vec{\varphi}\,dx = \int_\Omega \vec{f}\cdot\vec{\varphi}\,dx.$$

We choose an approximating sequence of test functions $(\vec{\varphi}_h) \in V_h$ with $\vec{\varphi}_h \overset{H_0^1}{\to} \vec{\varphi}$, which are not divergence-free, but converge strongly in $[H_0^1(\Omega)]^d$ to the divergence-free function $\vec{\varphi}$. Since we can construct such a sequence by Lagrange interpolation, we can further assume that the norms $\|\vec{\varphi}_h\|_{L^\infty(\Omega)}$ and $\|\nabla\vec{\varphi}_h\|_{L^\infty(\Omega)}$ converge to $\|\vec{\varphi}\|_{L^\infty(\Omega)}$ and $\|\nabla\vec{\varphi}\|_{L^\infty(\Omega)}$, and are uniformly bounded.

The discrete solution $\vec{v}_h$ fulfills

$$\int_\Omega (\vec{v}_h\cdot\nabla)\vec{v}_h\cdot\vec{\varphi}_h\,dx - \int_\Omega p_h\nabla\cdot\vec{\varphi}_h\,dx + \int_\Omega \eta\nabla\vec{v}_h : \nabla\vec{\varphi}_h\,dx = \int_\Omega \vec{f}\cdot\vec{\varphi}_h\,dx.$$

For the right hand side holds

$$\lim_{h\to 0}\int_\Omega \vec{f}\cdot\vec{\varphi}_h\,dx = \int_\Omega \vec{f}\cdot\vec{\varphi}\,dx,$$

since $\vec{\varphi}_h$ converges strongly in $[L^2(\Omega)]^d$ to $\vec{\varphi}$.

Similarly, we obtain

$$\lim_{h\to 0}\int_\Omega \eta\nabla\vec{v}_h : \nabla\vec{\varphi}_h\,dx = \int_\Omega \eta\nabla\vec{v} : \nabla\vec{\varphi}\,dx,$$

since $\vec{\varphi}_h$ converges strongly in $[H_0^1(\Omega)]^d$ to $\vec{\varphi}$, and $\vec{v}_h$ converges weakly in $[H_0^1(\Omega)]^d$ to $\vec{v}$. The result follows by weak-strong convergence of the entire integral.

For the distributional pressure gradient we recall that p_h is uniformly bounded by

$$\|p_h\|_0 \le \frac{1}{\beta_h}\left(\left\|\vec{f}\right\| + \eta\,\|\nabla\vec{v}_h\|_0 + c\,\|\nabla\vec{v}_h\|_0^2\right) \le C,$$

where β_h is the discrete LBB constant of the Scott-Vogelius element. Therefore, we obtain

$$\left|\int_\Omega p_h\nabla\cdot\vec{\varphi}_h\,dx\right| \le C\,\|\nabla\cdot\vec{\varphi}_h\|_0 \to 0,$$

for $h \to 0$.

For the nonlinear term we adapt the argument from [28]. The identity

$$\int_\Omega (\vec{v}_h\cdot\nabla)\vec{v}_h\cdot\vec{\varphi}_h\,dx = -\int_\Omega (\vec{v}_h\cdot\nabla)\vec{\varphi}_h\cdot\vec{v}_h\,dx$$

holds, and since $\nabla\vec{\varphi}_h$ is bounded by assumption and $\vec{v}_h$ converges strongly in $[L^2(\Omega)]^d$ to $\vec{v}$, we obtain finally

$$\lim_{h\to 0}\int_\Omega (\vec{v}_h\cdot\nabla)\vec{v}_h\cdot\vec{\varphi}_h\,dx = \int_\Omega (\vec{v}\cdot\nabla)\vec{v}\cdot\vec{\varphi}\,dx.$$

Therefore, for the weak limit $\vec{v}$ holds

$$\int_\Omega (\vec{v}\cdot\nabla)\vec{v}\cdot\vec{\varphi}\,dx + \int_\Omega \eta\nabla\vec{v} : \nabla\vec{\varphi}\,dx = \int_\Omega \vec{f}\cdot\vec{\varphi}\,dx,$$

i.e., it is indeed a solution of the steady Navier-Stokes equations. Finally, we obtain for $\|\nabla\vec{v}_h\|_0$

$$\lim_{h\to 0}\eta\,\|\nabla\vec{v}_h\|_0^2 = \lim_{h\to 0}\int_\Omega \vec{f}\cdot\vec{\varphi}_h\,dx = \int_\Omega \vec{f}\cdot\vec{\varphi}\,dx = \eta\,\|\nabla\vec{v}\|_0^2,$$

and from the weak convergence $\vec{v}_h \overset{H_0^1}{\rightharpoonup} \vec{v}$, together with the norm convergence $\|\nabla\vec{v}_h\|_0 \to \|\nabla\vec{v}\|_0$ follows also the strong convergence $\vec{v}_h \overset{H_0^1}{\to} \vec{v}$. □

3.3.2 Convergence of the convection-diffusion equation

Essential for the convergence proof of the coupled scheme is the definition of two reconstructions of the vector $\vec{v}_h$ on the Voronoi grid $\mathscr{V}_h$ similar to the definition of the scaled velocity (3.4) in the discretization of the coupled scheme. First, we define the vector $\vec{v}_{h,vol}$, which is constant on each diamond D_σ and its value is given by the volume average of $\vec{v}_h$ on D_σ, i.e.,

$$\vec{v}_{h,\mathrm{vol}}|_{D_\sigma} = \frac{1}{|D_\sigma|}\int_{D_\sigma}\vec{v}_h\,dx. \tag{3.15}$$

Second, we define the vector $\vec{v}_{h,\mathrm{face}}$, which is also constant on each diamond D_σ, but its value is given by the face average of $\vec{v}_h$ on σ, i.e.,

$$\vec{v}_{h,\mathrm{face}}|_{D_\sigma} = \frac{1}{|\sigma|}\int_\sigma \vec{v}_h ds. \tag{3.16}$$

For these reconstructions, the following results hold:

Lemma 3.3. *For any sequence $(\vec{v}_h) \in [H_0^1(\Omega)]^d$ which converges strongly in $[H^1(\Omega)]^d$ to some $\vec{v} \in [H_0^1(\Omega)]^d$, the sequences $(\vec{v}_{h,\mathrm{vol}})$ and $(\vec{v}_{h,\mathrm{face}})$ converge strongly in $[L^2(\Omega)]^d$ to $\vec{v}$.*

Proof. The strong L^2-convergence of $\vec{v}_{h,\mathrm{vol}}$ to $\vec{v}$ is obvious. The convergence of $\vec{v}_{h,\mathrm{face}}$ can be traced back to the convergence of $\vec{v}_{h,\mathrm{vol}}$ by

$$\left\|\vec{v}_{h,\mathrm{face}} - \vec{v}\right\|_0 \le \left\|\vec{v}_{h,\mathrm{face}} - \vec{v}_{h,\mathrm{vol}}\right\|_0 + \left\|\vec{v}_{h,\mathrm{vol}} - \vec{v}\right\|_0.$$

We obtain

$$\begin{aligned}\left\|\vec{v}_{h,\mathrm{face}} - \vec{v}_{h,\mathrm{vol}}\right\|_0^2 &= \sum_{\sigma\in\mathscr{E}} |D_\sigma| \left(\frac{1}{|\sigma|}\int_\sigma \vec{v}_h ds - \frac{1}{|D_\sigma|}\int_{D_\sigma}\vec{v}_h\,dx\right)^2 \\ &\le C\sum_{\sigma\in\mathscr{E}} |D_\sigma|\frac{h_\sigma}{|\sigma|}\int_{D_\sigma}\|\nabla\vec{v}_h\|_0^2\,dx,\end{aligned}$$

which is true according to [8], pp. 777. Moreover, the constant C does depend only on the regularity of the Voronoi grid $\mathscr{V}_h$. Using $|D_\sigma| = \frac{|\sigma| h_\sigma}{d}$, we obtain finally

$$\left\| \vec{v}_{h,\text{face}} - \vec{v}_{h,\text{vol}} \right\|_0 \leq Ch \left\| \nabla \vec{v}_h \right\|_0,$$

and $\vec{v}_{h,\text{face}}$ converges strongly in $[L^2(\Omega)]^d$ to $\vec{v}$. □

A special, piecewise constant reconstruction on diamonds for gradients is also fundamental for the convergence proof.

Lemma 3.4. *For a function $\varphi \in C_0^\infty(\Omega)$, we define a reconstruction $\nabla_h \varphi$ of its gradient $\nabla \varphi$ on a diamond D_σ for $\sigma = K|L$ by*

$$\nabla_h \varphi_{|D_\sigma} = d \frac{\varphi(\vec{x}_L) - \varphi(\vec{x}_K)}{d_{KL}} \cdot \vec{n}_{KL},$$

for $\vec{n}_{KL} := \vec{h}_{KL}/d_{KL}$. This discrete gradient converges to $\nabla \varphi \in [L^\infty(\Omega)]^d$ in the weak topology, i.e., for every function $\vec{f} \in [L^1(\Omega)]^d$ holds*

$$\int_\Omega \vec{f} \cdot \nabla_h \varphi \, dx \to \int_\Omega \vec{f} \cdot \nabla \varphi \, dx.$$

Proof. For this result in the convergence theory for finite volume methods, we refer to [8]. □

For $\varphi \in C_0^\infty(\Omega)$, we multiply the left hand side of the finite volume scheme (3.6) with $\varphi_K = \varphi(\vec{x}_K)$ and sum over all control volumes. Using

$$g(c_L, c_K, v) = -g(c_K, c_L, -v),$$

which is due to (3.7), we obtain

$$\sum_{K \in \mathscr{K}} \varphi_K \sum_{L \in \mathscr{N}_K} \tau_{KL} g(c_K, c_L, v_{\sigma_{KL}}) = \sum_{K|L \in \mathscr{E}} \tau_{KL} g(c_K, c_L, v_{\sigma_{KL}}) (\varphi_K - \varphi_L) \quad =: a_h(c_h, \varphi_h) \tag{3.17}$$

We introduce the space $W_h^0 = \left\{ c_h \in W_h | \, c_{h|K} = 0 \, \forall K \in \mathscr{K}_I \right\}$. We obtain an equivalent description of (3.6) for the homogeneous Dirichlet case: Find $c_h \in W_h^0$ such that

$$a_h(c_h, \varphi_h) = \sum_{K \in \mathscr{K}} |K| s_K \varphi_K \tag{3.18}$$

holds for all test functions $\varphi_h \in W_h^0$.

The convergence proof relies heavily on the proof given in [8]. Therefore, we will only sketch it. We will focus mainly on the points, where we have slightly different arguments. The natural norm for the space W_h^0 is defined as the following discrete gradient norm

$$\|c_h\|_{1,h} := \left(\sum_{K|L \in \mathscr{E}} \tau_{KL} (c_K - c_L)^2 \right)^{\frac{1}{2}}.$$

Lemma 3.5 (Existence and uniqueness of a discrete solution)**.** *The finite volume scheme* (3.6) *has a unique solution on every boundary conforming Delaunay grid.*

Proof. Existence and uniqueness of the scheme will be proved by demonstrating the coercivity of the discrete bilinear form a_h in (3.17). Therefore, we test the bilinear form a_h with $\varphi_h := c_h \in W_h^0$ and obtain

$$\begin{aligned} a_h(c_h, c_h) = \\ \sum_{K|L\in\mathscr{E}} \tau_{KL}\, g(c_K, c_L, v_{\sigma_{KL}})\,(c_K - c_L) = \\ \sum_{K|L\in\mathscr{E}} \tau_{KL} \left(DU_{\text{even}}\left(\frac{v_{\sigma_{KL}}}{D}\right)(c_K - c_L) + \frac{c_K + c_L}{2} v_{\sigma_{KL}} \right)(c_K - c_L) = \\ \sum_{K|L\in\mathscr{E}} \tau_{KL} \left(DU_{\text{even}}\left(\frac{v_{\sigma_{KL}}}{D}\right)(c_K - c_L)^2 + \frac{c_K^2 - c_L^2}{2} v_{\sigma_{KL}} \right) \geq \\ D \sum_{K|L\in\mathscr{E}} \tau_{KL}\,(c_K - c_L)^2 + \sum_{K\in\mathscr{K}} c_K^2 \sum_{L\in\mathscr{N}_K} \tau_{KL} v_{\sigma_{KL}} = D\,\|c_h\|_{1,h}^2 . \end{aligned}$$

The last estimate holds, since we have $U_{\text{even}}(z) \geq 1$, and the velocity projections $v_{\sigma_{KL}}$ are discretely divergence-free. □

Lemma 3.6 (Stability and weak convergence)**.** *We assume that* $(\vec{v}_h, c_h)$ *is a sequence of discrete solutions of* (3.1) *and* (3.6) *such that the sequence* $(\vec{v}_h)$ *converges strongly in* $[H_0^1(\Omega)]^d$ *to a solution* $\vec{v}$ *of* (2.4)*. Then, from the sequence* (c_h) *we can extract a subsequence which converges strongly in* $L^2(\Omega)$ *to some* $c \in H_0^1(\Omega)$*.*

Proof. Again, testing the scheme (3.17) by $\varphi_h := c_h$ yields

$$D\,\|c_h\|_{1,h}^2 \leq \sum_{K|L\in\mathscr{E}} \tau_{KL}\, g(c_K, c_L, v_{\sigma_{KL}})\,(c_K - c_L) = \sum_{K\in\mathscr{K}} |K| s_K c_K .$$

By the Cauchy-Schwarz and the discrete Poincaré inequalities, see [8], we obtain the uniform stability estimate

$$\|c_h\|_{1,h} \leq \frac{\operatorname{diam}(\Omega)}{D}\,\|s\|_0 .$$

By a discrete version of Rellich's theorem [9] we conclude that a subsequence of (c_h) converges strongly in L^2 to some $c \in H_0^1(\Omega)$. □

Theorem 3.2 (Convergence of the coupled scheme)**.** *We assume that* $(\vec{v}_h, c_h)$ *is a sequence of discrete solutions of* (3.1) *and* (3.6) *such that* $(\vec{v}_h)$ *converges strongly in* $[H_0^1(\Omega)]^d$ *to a solution* $\vec{v}$ *of* (2.4)*, and such that a subsequence of* (c_h) *converges strongly in* L^2 *to some* $c \in H_0^1(\Omega)$ *according to Lemma 3.6. Then, the accumulation point* $c \in H_0^1(\Omega)$ *of* (c_h) *is the unique solution of the continuous problem* (2.5)*, where the solution* $\vec{v}$ *of* (2.4) *drives the convection. Therefore, also the entire sequence* (c_h) *from Lemma 3.6 converges strongly in* L^2 *to the unique* c*, and not only a subsequence.*

Proof. In the following, we denote the subsequence of (c_h) also as (c_h). For the proof we choose an arbitrary test function $\varphi \in C_0^\infty(\Omega)$ and use a projection of $\varphi_h \in W_h^0$ onto the Delaunay grid as a discrete test function, i.e., we have $\varphi_{h|K} = \varphi_K = \varphi(\vec{x}_K)$. Then, we obtain for the right hand side of the discrete scheme (3.17) that

$$\lim_{h\to 0} \sum_{K\in\mathscr{K}_h} |K| s_K \varphi_K \to \int_\Omega s\varphi \, dx,$$

since (s_K) and φ_h converge strongly in L^2 to s and φ.

Now, we investigate the convergence of the discrete diffusion in (3.17)

$$\begin{aligned} T_{\text{diffusive}} &:= D \sum_{K|L\in\mathscr{E}} \tau_{KL} U_{\text{even}}\left(\frac{v_{\sigma_{KL}}}{D}\right)(c_K - c_L)(\varphi_K - \varphi_L) \\ &= D \sum_{K|L\in\mathscr{E}} \tau_{KL}(c_K - c_L)(\varphi_K - \varphi_L) \\ &\qquad + D \sum_{K|L\in\mathscr{E}} \tau_{KL}\left(U_{\text{even}}\left(\frac{|v_{\sigma_{KL}}|}{D}\right) - 1\right)(c_K - c_L)(\varphi_K - \varphi_L) \\ &=: T_{\text{natdiff}} + T_{\text{artdiff}}, \end{aligned}$$

where T_{natdiff} describes an approximation of the natural diffusion of the continuous problem and T_{artdiff} describes the artificial diffusion of the numerical scheme.

First, we investigate the behavior of T_{natdiff} for $h \to 0$, and introduce the consistency error of the diffusive flux

$$R_{KL} := \frac{1}{|\sigma_{KL}|}\int_{K|L} \nabla\varphi \cdot \vec{n}_{KL} ds - \frac{\varphi_L - \varphi_K}{d_{KL}}.$$

Since the discrete approximation of these directional gradients is first order accurate [8], we have an estimate for the consistency error by

$$|R_{KL}| \le C_\varphi h, \tag{3.19}$$

where C_φ depends on the regularity of φ and on the mesh regularity of the Voronoi grid, but not on the mesh size. We compute

$$\begin{aligned} \left| T_{\text{natdiff}} + \int_\Omega D c_h \Delta\varphi \, dx \right| &= \left| T_{\text{natdiff}} + \sum_{K\in\mathscr{K}} \int_K D c_h \Delta\varphi \, dx \right| \\ &= \left| T_{\text{natdiff}} + D \sum_{K|L\in\mathscr{E}} (c_K - c_L) \int_{K|L} \nabla\varphi \cdot \vec{n}_{KL} ds \right| \\ &= D \left| \sum_{K|L\in\mathscr{E}} \sigma_{KL}(c_K - c_L) R_{KL} \right| \\ &\le D \|c_h\|_{1,h} \left(\sum_{K|L\in\mathscr{E}} \sigma_{KL} d_{KL} R_{KL}^2 \right)^{\frac{1}{2}} \\ &\le D \|c_h\|_{1,h} d^{\frac{1}{2}} |\Omega|^{\frac{1}{2}} \max_{\sigma=K|L} |R_{KL}|. \end{aligned}$$

The estimate in the last line is due to (3.3). By (3.19), we now obtain that

$$\left| T_{\text{natdiff}} + D \int_\Omega c_h \Delta\varphi \, dx \right| \leq C_\varphi d^{\frac{1}{2}} |\Omega|^{\frac{1}{2}} \|s\|_0 h$$

holds, and we arrive at

$$\lim_{h\to 0} T_{\text{natdiff}} \to -D \lim_{h\to 0} \int_\Omega c_h \Delta\varphi \, dx = -D \int_\Omega c \, \Delta\varphi \, dx,$$

since c_h converges strongly in L^2 to c.

In the second step, we show that the artificial diffusion T_{artdiff} vanishes for $h \to 0$ in an appropriate sense. Due to the assumptions on $U_{\text{even}}(z)$ we have

$$\begin{aligned}
|T_{\text{artdiff}}| &= \left| D \sum_{K|L\in\mathscr{E}} \tau_{KL} \left(U_{\text{even}}\left(\frac{|v_{\sigma_{KL}}|}{D} \right) - 1 \right) (c_K - c_L)(\varphi_K - \varphi_L) \right| \\
&\leq \left| \sum_{K|L\in\mathscr{E}} \tau_{KL} \frac{|v_{\sigma_{KL}}|}{2} (c_K - c_L)(\varphi_K - \varphi_L) \right| \\
&\leq \left| \sum_{K|L\in\mathscr{E}} \frac{\sigma_{KL} d_{KL}}{2} |v_{\sigma_{KL}}| \frac{c_K - c_L}{d_{KL}} \frac{\varphi_K - \varphi_L}{d_{KL}} \right| \\
&\leq \|\nabla\varphi\|_{L^\infty(\Omega)} \sum_{K|L\in\mathscr{E}} \frac{\sigma_{KL} d_{KL}}{2} |v_{\sigma_{KL}}| \frac{|c_K - c_L|}{d_{KL}} \\
&\leq \frac{1}{2} \|\nabla\varphi\|_{L^\infty(\Omega)} \|c_h\|_{1,h} \left(\sum_{K|L\in\mathscr{E}} \sigma_{KL} d_{KL} |v_{\sigma_{KL}}|^2 \right)^{\frac{1}{2}}.
\end{aligned}$$

Since $\|\nabla\varphi\|_{L^\infty}$ and $\|c_h\|_{1,h}$ are bounded, we have to show that the last term in the last line converges to zero for $h \to 0$. We estimate it by

$$\begin{aligned}
\sum_{K|L\in\mathscr{E}} \sigma_{KL} d_{KL} |v_{\sigma_{KL}}|^2 &= \sum_{K|L\in\mathscr{E}} \sigma_{KL} d_{KL} \left| \frac{v_{\sigma_{KL}}}{d_{KL}} \right|^2 d_{KL}^2 \\
&= \sum_{K|L\in\mathscr{E}} \sigma_{KL} d_{KL} |\vec{v}_{h,\text{face}} \cdot \vec{n}_{KL}|^2 d_{KL}^2 \\
&\leq \sum_{K|L\in\mathscr{E}} \sigma_{KL} d_{KL} |\vec{v}_{h,\text{face}}|^2 d_{KL}^2 \\
&\leq d h^2 \left\| \vec{v}_{h,\text{face}} \right\|_0^2. \qquad (3.20)
\end{aligned}$$

Since $\left\| \vec{v}_{h,\text{face}} \right\|_0$ converges to $\|\vec{v}\|_0$ for $h \to 0$ according to Lemma 3.3, we obtain that the contribution of the artificial diffusion T_{artdiff} indeed vanishes for $h \to 0$.

In the last step, we investigate the convergence of the discrete convection in (3.17). We

define

$$\begin{aligned}
T_{\text{convective}} &:= D \sum_{K|L\in\mathscr{E}} \tau_{KL} U_{\text{odd}}\Big(\frac{v_{\sigma_{KL}}}{D}\Big)\,(c_K + c_L)\,(\varphi_K - \varphi_L) \\
&= \sum_{K|L\in\mathscr{E}} \tau_{KL} \frac{c_K + c_L}{2} v_{\sigma_{KL}}\,(\varphi_K - \varphi_L) \\
&= \sum_{K\in\mathscr{K}} \varphi_K \sum_{L\in\mathscr{N}(K)} \tau_{KL} \frac{c_K + c_L}{2} v_{\sigma_{KL}} \\
&= \sum_{K\in\mathscr{K}} \varphi_K \sum_{L\in\mathscr{N}(K)} \tau_{KL} \frac{c_K + c_L}{2} v_{\sigma_{KL}} - \sum_{K\in\mathscr{K}} \varphi_K \sum_{L\in\mathscr{N}(K)} \tau_{KL} c_K v_{\sigma_{KL}},
\end{aligned}$$

because $(v_\sigma)_\sigma$ is discretely divergence-free. Therefore, we obtain

$$\begin{aligned}
T_{\text{convective}} &= \sum_{K\in\mathscr{K}} \varphi_K \sum_{L\in\mathscr{N}(K)} \tau_{KL} \frac{c_L - c_K}{2} v_{\sigma_{KL}} \\
&= -\sum_{K|L\in\mathscr{E}} \tau_{KL} \frac{c_K - c_L}{2} v_{\sigma_{KL}}\,(\varphi_K - \varphi_L) \\
&= -\sum_{K\in\mathscr{K}} c_K \sum_{L\in\mathscr{N}(K)} \left(\frac{\sigma_{KL} d_{KL}}{2d}\right) \frac{v_{\sigma_{KL}}}{d_{KL}} \left(d\frac{\varphi_K - \varphi_L}{d_{KL}}\right) \\
&= -\int_\Omega c_h \vec{v}_{h,\text{face}} \cdot \nabla_h \varphi \, dx
\end{aligned}$$

Now, c_h converges strongly to c in L^2, and $\vec{v}_{h,\text{face}}$ converges strongly to $\vec{v}$ in $[L^2(\Omega)]^d$ according to Lemma 3.3. Therefore, $c_h\vec{v}_{h,\text{face}}$ converges strongly to $c\vec{v}$ in $[L^1(\Omega)]^d$. Further, according to Lemma 3.4 we have weak* convergence of $\nabla_h\varphi$ to $\nabla\varphi \in [L^\infty(\Omega)]^d$, and finally

$$\lim_{h\to 0} -\int_\Omega c_h \vec{v}_{h,\text{face}} \cdot \nabla_h \varphi \, dx = -\int_\Omega c\vec{v} \cdot \nabla\varphi \, dx$$

holds, i.e.,

$$T_{\text{convective}} \to -\int_\Omega c\vec{v} \cdot \nabla\varphi \, dx.$$

Now we can conclude that the accumulation point $c \in H_0^1(\Omega)$ fulfills the equation

$$-D\int_\Omega c\,\Delta\varphi \, dx - \int_\Omega c\,\vec{v} \cdot \nabla\varphi \, dx = \int_\Omega s\varphi \, dx$$

for all $\varphi \in C_0^\infty(\Omega)$ and it is the unique solution of (2.5). Further, for a given velocity solution $\vec{v}$ of the steady Navier-Stokes equations, the entire sequence (c_h) converges, since every accumulation point of (c_h) is the unique limit c. □

Remark 3.1. *When it is known a-priori that $\vec{v}$ has the regularity $H_0^1 \cap L^\infty$, then the convergence proof can be simplified, since the local Péclet number $\frac{|v_{\sigma_{KL}}|}{D}$ vanishes uniformly in this case. In the general case, the local Péclet number can exceed every bound, but the L^2 norm of the local Péclet number vanishes, see* (3.20).

Of course, the artificial diffusion is entirely zero for the central difference approximation of the convection, i.e., for $U(z) = U_{\text{dcd}}(z)$, and then this issue does not exist, either.

Remark 3.2. *When, in addition, it is known a-priori that $\vec{v}$ is continuous, then the proof becomes even simpler, because then the strong convergence $\vec{v}_{h,\mathrm{face}} \to \vec{v}$ in $[L^2(\Omega)]^d$ is trivial.*

4 Boundary fluxes and maximum principles

4.1 Calculation of the anode fluxes

The application below of the proposed coupling scheme requires the accurate computation of the total current over the anode, which is given by

$$Q_A := \int_{\Gamma_A} \vec{q} \cdot \vec{n} ds.$$

For $s \in L^2(\Omega)$, the flux $\vec{q}$ is in $[L^2(\Omega)]^d$, and also its divergence is in $L^2(\Omega)$. Therefore, we can apply the Gauss theorem, in order to replace the integral over the surface by a volume integral using appropriate test functions. Let $T \in H^1(\Omega)$ be a test function such that

$$T|_{\Gamma_A} = 1, \quad T|_{\Gamma_I} = 0, \quad T|_{\Gamma_O} = 0 \tag{4.1}$$

E.g., T can be the weak solution of a Laplace problem with the corresponding Dirichlet boundary conditions, and we then obtain

$$\begin{aligned} Q_A &= \int_{\Gamma_A} T\vec{q} \cdot \vec{n} ds + \int_{\Gamma_W} T\vec{q} \cdot \vec{n} ds + \int_{\Gamma_I} T\vec{q} \cdot \vec{n} ds + \int_{\Gamma_O} T\vec{q} \cdot \vec{n} ds \\ &= \int_{\Gamma} T\vec{q} \cdot \vec{n} ds = \int_{\Omega} \nabla \cdot (T\vec{q}) dx = \int_{\Omega} \nabla T \cdot \vec{q} dx + \int_{\Omega} T s dx. \end{aligned}$$

Remark 4.1. *Similar procedures can be used to calculate the fluxes q_I, q_O through the inflow and outflow boundaries. Choosing as particular test functions the weak solutions T_A, T_I, T_O of the corresponding Laplace equations, one establishes that $T_A + T_I + T_O = 1$ which implies the physically meaningful flux balance*

$$q_A + q_I + q_O = 0. \tag{4.2}$$

Now the calculation of the discrete fluxes follows:

Lemma 4.1 (Definition and convergence of discrete boundary flux integrals)**.** *Let $T_h \in W_h$ be a discrete test function fulfilling* (4.1)*. Define the weak discrete flux as*

$$q_{A,h} = \sum_{K|L \in \mathscr{E}} \frac{\tau_{KL}}{d_{KL}} (T_K - T_L) g_{KL}(c_k, c_K, v_{\sigma_{KL}})$$

Then, we have

$$\lim_{h \to 0} q_{A,h} = q_A.$$

Proof. We choose $T \in C^\infty(\Omega)$ fulfilling (4.1) and set $T_{h,K} = T(\vec{x}_K)$ which then fulfills the discrete equivalent of (4.1). Then the convergence of the flux integral follows from weak-strong convergence in a similar way, as above. For that, we must interpret the discrete sum as an integral over the product of strongly converging approximations to ∇T, and weakly converging approximations of $\vec{q}$. □

4.2 Maximum principles

In order to illustrate the significance of the incompressibility of the vector field $\vec{v}$ in (2.5) for maximum principles and the role of the outflow boundary conditions, we give a short proof for weakly differentiable species concentrations. The approach is based on considerations in [17, 7]. For the corresponding discrete results including the introduction of the outflow boundary conditions, we refer to [11].

Lemma 4.2.

1 *Global minimax principle:* $0 \leq c \leq c_I$ *a.e.*

2 *Local minimax principle: For almost every* $x \in \Omega$ *and any neighborhood* $B \subset \Omega$ *containing* x*,*

$$\operatorname{ess}\inf_{\partial B} c \leq c(x) \leq \operatorname{ess}\sup_{\partial B} c$$

Proof. Let $w = (c-k)^+, \Rightarrow (c-k)^+ \in H^1_D$ where $k = \sup c_d$. Then, we have

$$\begin{aligned}
0 &= \int_\Omega (D\nabla c - \vec{v}c)\cdot\nabla(c-k)^+ dx + \int_{\Gamma_O} \vec{v}\cdot\vec{n}c(c-k)^+ ds \\
&= \int_\Omega (D\nabla(c-k)^+ - \vec{v}(c-k)^+)\cdot\nabla(c-k)^+ dx + \int_{\Gamma_O} \vec{v}\cdot\vec{n}(c-k)^+(c-k)^+ ds \\
&- k\int_\Omega \vec{v}\cdot\nabla(c-k)^+ dx + k\int_{\Gamma_O} \vec{v}\cdot\vec{n}(c-k)^+ \\
&= \int_\Omega (D\nabla(c-k)^+ - \vec{v}(c-k)^+)\cdot\nabla(c-k)^+ dx + \int_{\Gamma_O} \vec{v}\cdot\vec{n}(c-k)^+(c-k)^+ ds - k\int_\Omega (c-k)^+\nabla\cdot\vec{v}\, dx \\
&\geq \mu||(c-k)^+||^2
\end{aligned}$$

due to coercivity, divergence-free $\vec{v}$, and boundary conditions for c and $\vec{v}$. Therefore, $(x-k)^+ = 0$ and $c \leq k$. We remark that this maximum principle includes the bounds of the values on the outflow boundary as well. For the minimum part, reasoning is similar.

The local maximum principle is derived from the fact that on a subdomain B, we can derive a boundary value problem with Dirichlet boundary conditions for which in turn, the global maximum principle applies. □

Lemma 4.3 (A-priori estimate and local maximum principle for the finite volume solution)**.** *For any solution* $(c_K)_{K\in\mathscr{K}}$ *of the discrete problem* (3.6) *with* $(s_K) = 0$*, we have the following estimates:*

1 Global minimax principle:

$$0 \leq c_K \leq c_I \quad \forall K \in \mathscr{K} \tag{4.3}$$

2 Local minimax principle:

$$\min_{L \in \mathscr{N}_K} c_L \leq c_K \leq \max_{L \in \mathscr{N}_K} c_L \quad \forall K \in \mathscr{K}^0 \tag{4.4}$$

Proof. According to (3.6)

$$\begin{aligned}
0 &= \sum_{L \in \mathscr{N}_K} \tau_{KL} g(c_K, c_L, v_{\sigma_{KL}}) + \sum_{\sigma \in \mathscr{G}_K^O} \tau_\sigma g(c_K, c_K, v_\sigma) \\
&= \sum_{L \in \mathscr{N}_K} \tau_{KL} \left(g(c_K, c_L, v_{\sigma_{KL}}) - g(c_K, c_K, v_{\sigma_{KL}}) \right) + \sum_{L \in \mathscr{N}_K} \tau_{KL} g(c_K, c_K, v_{\sigma_{KL}}) + \sum_{\sigma \in \mathscr{G}_K^O} \tau_\sigma g(c_K, c_K, v_\sigma) \\
&= \sum_{L \in \mathscr{N}_K} \tau_{KL} DU\left(-\frac{v_{\sigma_{KL}}}{D} \right) (c_K - c_L) + \sum_{L \in \mathscr{N}_K} \tau_{KL} v_{\sigma_{KL}} + \sum_{\sigma \in \mathscr{G}_K^O} \tau_\sigma v_\sigma \\
&= c_K \sum_{L \in \mathscr{N}_K} \tau_{KL} DU\left(-\frac{v_{\sigma_{KL}}}{D} \right) - \sum_{L \in \mathscr{N}_K} \tau_{KL} DU\left(-\frac{v_{\sigma_{KL}}}{D} \right) c_L
\end{aligned}$$

Therefore $c_K = \sum_{L \in \mathscr{N}_K} \xi_{KL} c_L$ with

$$0 < \xi_{KL} = \frac{\tau_{KL} U\left(-\frac{v_{\sigma_{KL}}}{D} \right)}{\sum_{M \in \mathscr{N}_K} \tau_{KM} U\left(-\frac{v_{\sigma_{KM}}}{D} \right)} < 1$$

and $\sum_{L \in \mathscr{N}_K} \xi_{KL} = 1$, resulting in (ii). (i) is easily derived from (ii). □

Lemma 4.4. *The discretization matrix has the M-Property.*

Proof. The system matrix is easily derived from (3.6). As the domain Ω is connected, the graph of the matrix consisting of the edges with $\tau_{KL} > 0$ is connected. Upwinding ensures positivity of main diagonal entries and nonnegativity of the off diagonal entries. Due to the existence of at least one Dirichlet node, from the proof of previous lemma, we derive weak diagonal dominance, see also [11]. □

Finite element assembly for the Navier-Stokes equation has been implemented in Alberta [22]. Finite volume assembly has been implemented in pdelib2 [27]. The solution of the linear systems has been done with Pardiso [21]. In the sequel, we elaborate on particular issues of the presented method.

4.3 Mesh generation

Mesh generation is essential to the numerical approach we have chosen. Besides the necessity to fit into the given geometry, the proposed method depends on the availability of meshes with certain properties.

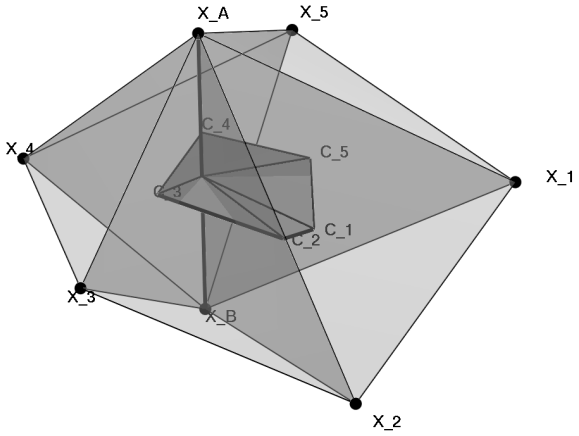

Figure 2: Voronoi box facet corresponding to the interior edge $X_A X_B$. It is planar and the convex hull of the circumcenters C_i of the tetrahedra surrounding this edge spanned by points X_A, X_B, X_i, X_{i+1}, respectively. A canonical triangulation of this facet is obtained using the edge midpoint as a common vertex. Note that the circumcenter C_2 of the tetrahedron X_A, X_B, X_2, X_3 lies outside its defining tetrahedron, nevertheless the Voronoi box facet and its triangulation can be obtained due to the Delaunay property.

In order to allow the definition of the Voronoi-box based finite volume method, the finite volume simplex mesh has to have the boundary conforming Delaunay property [26]. Furthermore, as in [13], it is necessary to resolve the boundary layer at the anode, such that the grid becomes anisotropic close to the electrode, and the main directions of anisotropy are aligned with the normal resp. tangential directions of the electrode surface. As three-dimensional state-of-the-art mesh generators [23, 25] are not able to fulfill this demand in an automatic fashion, we have chosen the following approach: a two-dimensional boundary conforming Delaunay grid is created using the mesh generator TRIANGLE [24]. Using this as a base, a prismatic grid with adaptive spacing in the direction orthogonal to the anode is created, from which all elements not corresponding to the geometry are removed. Finally, the prisms are subdivided into tetrahedra, resulting in a three-dimensional boundary conforming Delaunay grid.

Due to its higher order, for the mixed finite element method, we use a coarser grid than for the calculation of the concentration profile. In order to be able to apply the Scott-Vogelius element in this case, each tetrahedron is subdivided into four tetrahedra by adding its barycenter.

5 Implementation issues

5.1 Practical realization of the coupling scheme

So far, it was only stated that coupling is realized by the calculation of the flux projections (3.4). While this seems simple and obvious, the implementation of this coupling

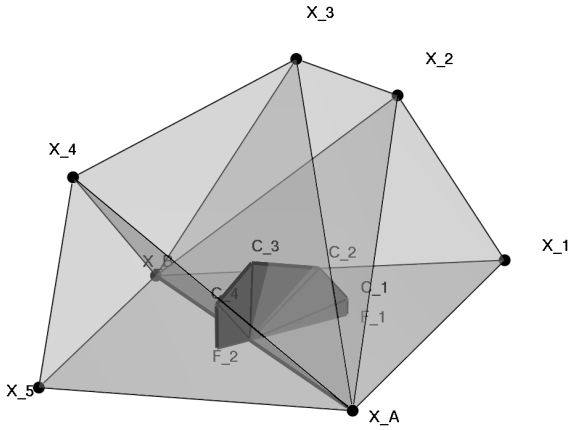

Figure 3: Voronoi box facet corresponding to the boundary edge $X_A X_B$ shared by the boundary triangles $X_A X_B X_1$ and $X_A X_B X_5$. It is planar and the convex hull of the circumcenters F_i of these two triangles and C_i of the tetrahedra surrounding this edge spanned by points X_A, X_B, X_i, X_{i+1}, respectively. A canonical triangulation of this facet is obtained using the edge midpoint as a common vertex. The fact that all tetrahedron circumcenters lie inside the domain is due to boundary conformality.

scheme is connected with considerable technical effort. For the sake of the completeness of the paper, we provide these algorithmic issues with some detail.

5.1.1 Calculation of the Voronoi diagram

The usual way to implement the Voronoi finite volume scheme is based on an assembly loop similar to that of a finite element method. For each simplex in the mesh, the local contributions to the system matrix are calculated locally and added into the corresponding entries of the global matrix. If the calculation of the flux integrals (3.4) is not necessary, only the edge length and area of the Voronoi surface are needed.

In the present case it is necessary to explicitely calculate the Voronoi surfaces. As this is connected with some technicalities at the boundaries, it is described here.

Let us assume to be given a boundary conforming Delaunay simplex mesh of the computational domain Ω. Assume $\Gamma = \partial\Omega = \bigcup_{i \in \mathscr{I}_\Gamma} \Gamma_i$ is the union of non-intersecting sections. Let $\mathscr{N}$ be the set of nodes of the partition and $\mathscr{E}$ the set of edges. Let $\mathscr{N}_I = \Omega \cap \mathscr{N}$ the set of interior nodes, and $\mathscr{N}_B = \Gamma \cap \mathscr{N}$ the set of boundary nodes.

The algorithm proceeds as follows:

1 For each interior edge, obtain the circumcenters of the simplices adjacent to it. The common facet of the Voronoi boxes corresponding to both endpoints of the edge is orthogonal to this edge and consists of the union of triangles which are generated by the edge midpoint and the respective circumcenters of two cells adjacent to the edge sharing a common face, see Fig. 2.

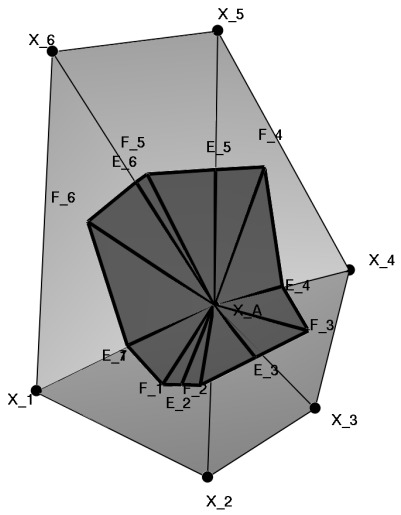

Figure 4: Voronoi box facets corresponding to the boundary node X_A. This part of the Voronoi box boundary is not necessarily planar. It is defined by the triangles $X_A F_i E_i$ and $X_A F_i E_{i+1}$ where F_i are the circumcenters of the triangles X_A, X_i, X_{i+1}, and E_i are the midpoints of the line $F_i F_{i+1}$ in the case the corresponding triangles are coplanar, or the midpoints of the edge $X_A X_i$, otherwise. This construction is forced by a case like that of the circumcenter F_2 which lies outside of its triangle. The line $X_1 X_A X_4$ separates different boundary conditions

2 For each boundary edge, obtain the circumcenters of the adjacent simplices and the two circumcenters of the adjacent boundary triangles. The common facet of the Voronoi boxes belonging to the both endpoints of the edge is orthogonal to this edge and contains as a subset the union of triangles which are generated by the edge midpoint and the respective circumcenters of two cells adjacent to the edge sharing a common face. In order to obtain the full facet, this union is joined by the two triangles set up by the edge circumcenter, one of the facet circumcenters and the simplex circumcenter of the simplex containing that face, see Fig. 3.

3 For each boundary node, obtain the adjacent boundary triangles. The intersection of the "raw" Voronoi box (which may extend to infinity) with the boundary consists of all triangles generated by the boundary node, one of the circumcenters of a triangle and a pseudo edge point corresponding to an edge of the triangle containing the boundary node. The pseudo edge point is defined as the edge midpoint if the two adjacent triangles are not coplanar or belong to different boundary conditions. Otherwise, the pseudo edge midpoint is calculated as the midpoint of the line connecting the circumcenters of the two triangles, see Fig. 4. The reason for this construction is that for coplanar triangles, the Delaunay condition allows a triangle circumcenter outside of the triangle if the corresponding edge does not belong to a different boundary condition.

4 For each boundary triangle, calculate the intersection with the boundary sections

Γ_i. After the previous construction, this intersection either is empty, or consists of the triangle itself.

As it consists of a fixed number of grid loops without search, this algorithm is $O(n)$. However in addition to the straightforward implementation, a number of additional incidence information needs to be generated in its course.

5.1.2 Calculation of the flux integrals

Given the Voronoi facets subdivided into triangles, in order to calculate the flux integrals (3.4), it remains to devise an algorithm to calculate the integrals over an arbitrary triangle contained in the domain. Therefore, we search all intersecting tetrahedra in the FEM mesh. Given a tetrahedron and a triangle in three-dimensional space, we obtain their intersection as the convex hull of the following points:

1 All triangle nodes contained in the tetrahedron

2 All tetrahedron edges intersecting the triangle

3 All triangle edges intersecting a tetrahedron face.

Using the mass center of this set of points as a common vertex, a triangulation of this convex set is readily obtained. The calculation of the point set needs two atomic operations: detection if a given point is located within a given simplex, and detection if a given line intersects a given triangle. These predicates are calculated with ε-accuracy allowing for false positives resulting in nearly zero area intersections. The flux integrals then are calculated on each subtriangle of the intersection using exact quadrature rules.

This approach allows for completely independent simplicial partitions for velocity and transport. The remaining challenge then is a proper search algorithm on which we will not elaborate.

6 Interpretation of a limiting current experiment

We report the results of [12] and discuss some issues.

The physical interpretation of the boundary conditions (2.3) is the calculation of the limiting current of a heterogeneous electrochemical reaction. The setting of the example discussed here is taken from [12].

At the inlet (Γ_I), a sulphuric acid (H_2SO_4) based electrolyte with given velocity profile $v_I(\vec{x})$ is injected with a concentration c_I of dissolved hydrogen H_2. At a certain potential applied between the anode Γ_A covered with a platinum catalyst, the part of the hydrogen reaching Γ_A reacts immediately according to

$$H_2 \rightarrow 2H^+ + 2e^-.$$

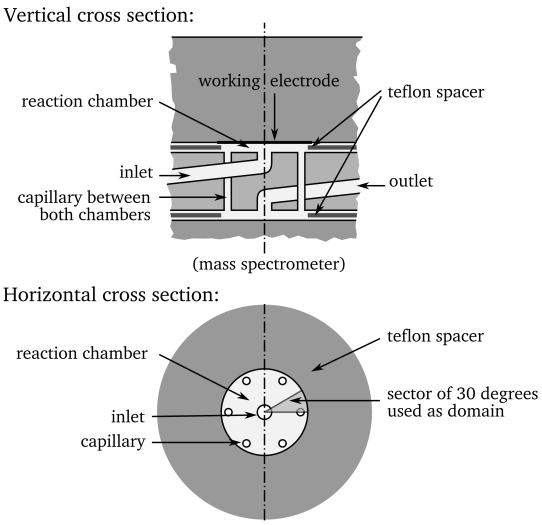

Figure 5: Schematic of a thin layer flow cell [16]. Diameter of working chamber: $6\ \mathrm{mm}$. Diameter of inlet: $1.0\ \mathrm{mm}$. Diameter of the six connecting capillaries between the two compartments: $0.5\ \mathrm{mm}$. By geometrical symmetry, the problem is reduced to the 30 degrees (gray) circular arc shown

The electrons e^- enter an external electrical circuit, and recombine with the protons H^+ at a counter electrode outside of the domain of consideration. The amount of H^+ generated during this reaction is marginal in comparison to the protons delivered with the electrolyte, and so we can assume that the reaction products "vanish" from the system. The flow containing the unreacted hydrogen leaves the cell at the outlet. Due to the assumed fast reaction, homogeneous Dirichlet boundaries are assumed at the anode Γ_A. The geometry is depicted in Figure 5. The symmetry of the cell allows to reduce the computational domain to one twelfth of the original problem. The anode current

$$I_E = 2F \int_{\Gamma_E} \frac{\partial c}{\partial \vec{n}} ds$$

is called the *limiting current*.

Experimental devices with special configurations which allow to avoid the calculation of the Navier-Stokes flow are well known by electrochemists [10] and have been modeled using the finite volume method discussed in the present paper in [13]. But cylindrical flow cells have the advantage that they can be rather easily manufactured, and they are well suited to the measurement on single crystal electrodes [12].

Corresponding to the experimental situation, calculations have been performed with varying inlet velocities.

Figures 6 and 7 show isosurfaces of the concentration in the volume and isolines of the concentration on the symmetry boundary for different velocities of the input which are all in the range of experimental measurements. We observe a transition between a

Figure 6: Concentration (in $\mathrm{mol}/\mathrm{m}^3$) for flow rates $0.5\ \mathrm{mm}^3/\mathrm{s}$ (left), $10\ \mathrm{mm}^3/\mathrm{s}$ (middle) and $80\ \mathrm{mm}^3/\mathrm{s}$ (right). Isosurfaces ($c = 1.0, 2.0 \ldots 6.0$) are shown in the interior of the working chamber. The anode is situated on the top. Isolines and grayscale color code at surfaces are shown at the inlet (left) and the outlet (right), and the bottom of the working chamber. For the purpose of better visualization, the graphical representation has been stretched by a factor around 10 in z direction compared to the original device.

prevalence of diffusion to a behavior with a Lévêque type boundary layer. The flow is discretized by the Scott-Vogelius element.

Figure 8 compares the concentration isosurfaces obtained with the Scott-Vogelius and Taylor-Hood Elements, respectively. We clearly see a striking difference concerning the maximum principle.

In order to give a more precise idea about the maximum principle, Figure 9 shows in the left the maximum concentration vs. flow rate for the different finite element discretizations. In the case of the Taylor-Hood element, we are unable to control the violation of the maximum principle. If we base the calculation on the Scott-Vogelius element, we see that the a-priori bound for the concentration given by the inlet velocity is observed.

The right plot in Figure 9 compares the values of the limiting current for different grids and discretizations with those measured in [29]. A first observation tells us that grid dependency of this value is well below the accuracy of the experimental data – in [12] it is discussed that the height of the cell is known with an accuracy around 30%, and differences in the cell height in this range influence the measured values far more

Figure 7: Concentration (in $\mathrm{mol}/\mathrm{m}^3$) for flow rates For the explanation of the visualization settings, see Fig. 6.

Figure 8: Concentration profile for flow rate $80mm^3/s$ on coarse grid: Scott-Vogelius (top) and Taylor-Hood (bottom). For the explanation of the visualization settings, see Fig. 6.

than the influence of the grid shown in Figure 9. At the same time one observes that the violation of the maximum principle does not significantly influence the value of the limiting current.

7 Acknowledgement

We acknowledge the support of the Deutsche Forschungsgemeinschaft in the frameworks of the Research Center MATHEON "Mathematics for Key Technologies" (project C23). Figures 6, 7, 8, 9 have been reproduced with permission by Elsevier Limited from [12].

References

[1] D. N. Allen and R. V. Southwell. Relaxation methods applied to determine the motion, in two dimensions, of a viscous fluid past a fixed cylinder. *Quart. J. Mech. and Appl. Math.*, 8:129–145, 1955.

[2] D. N. Arnold and J. Qin. Quadratic velocity/linear pressure Stokes elements. In R. Vichnevetsky, D. Knight, and G. Richter, editors, *Advances in Computer Methods for Partial Differential Equations VII*, pages 28–34. IMACS, 1992.

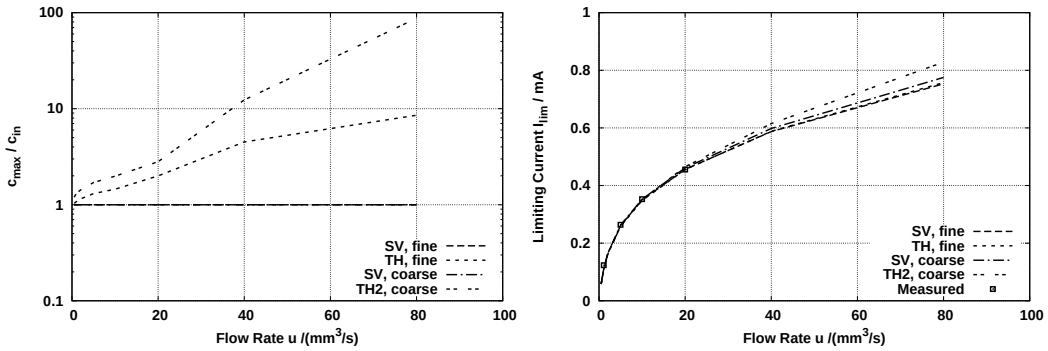

Figure 9: Maximum concentration vs. flow rate (left). Measured [29] and calculated limiting current for different grids and discretizations (right).

[3] F. Brezzi and M. Fortin. *Mixed and Hybrid Finite Elements*, volume 15 of *Springer Series in Computational Mathematics*. Springer, 1991.

[4] E. Burman and A. Linke. Stabilized finite element schemes for incompressible flow using Scott-Vogelius elements. *Appl. Numer. Math.*, 58(11):1704–1719, 2008.

[5] C. Calgaro, E. Creusé, and T. Goudon. An hybrid finite volume-finite element method for variable density incompressible flows. *J.Comp. Phys*, 227:4671–4696, 2008.

[6] P. G. Ciarlet. *The Finite Element Method for Elliptic Problems*, volume 4 of *Studies in Mathematics and its Applications*. North-Holland, 1978.

[7] M. Dobrowolski. *Angewandte Funktionalanalysis*. Springer, Berlin, 2009.

[8] R. Eymard, T. Gallouët, and R. Herbin. Finite volume methods. In *Handbook of numerical analysis, Vol. VII*, Handb. Numer. Anal., VII, pages 713–1020. North-Holland, Amsterdam, 2000.

[9] R. Eymard, T. Gallouët, R. Herbin, and J.-C. Latché. Analysis tools for finite volume schemes. *Acta Math. Univ. Comeniae*, 76(1):111–136, 2007.

[10] A. N. Frumkin, L. Nekrasov, V. G. Levich, and J. Ivanov. Die Anwendung der rotierenden Scheibenelectrode mit einem Ringe zur Untersuchung von Zwischenprodukten electrochemischer Reaktionen. *J. Electroanal. Chem*, 1:84–90, 1959.

[11] J. Fuhrmann and H. Langmach. Stability and existence of solutions of time-implicit finite volume schemes for viscous nonlinear conservation laws. *Appl. Numer. Math.*, 37(1–2):201–230, 2001.

[12] J. Fuhrmann, A. Linke, H. Langmach, and H. Baltruschat. Numerical calculation of the limiting current for a cylindrical thin layer flow cell. *Electrochimica Acta*, 55(2):430–438, 2009.

[13] J. Fuhrmann, H. Zhao, E. Holzbecher, H. Langmach, M. Chojak, R. Halseid, Z. Jusys, and R. Behm. Experimental and numerical model study of the limiting current in a channel flow cell with a circular electrode. *Phys. Chem. Chem. Phys.*, 10:3784 – 3795, 2008.

[14] V. John and P. Knobloch. On spurious oscillations at layers diminishing (SOLD) methods for convection-diffusion equations: Part I - a review. *Comp. Meth. Appl. Mech. Engrg.*, 196:2197–2215, 2007.

[15] V. John and P. Knobloch. On the performance of SOLD methods for convection-diffusion problems with interior layers. *Int. J. Comput. Sci. Math.*, 1(2-4):245–258, 2007.

[16] Z. Jusys, H. Massong, and H. Baltruschat. A new approach for simultaneous DEMS and EQCM: Electrooxidation of adsorbed CO on Pt and Pt-Ru. *J. Electrochem. Soc.*, pages 1093–1098, 1999.

[17] D. Kinderlehrer and G. Stampacchia. *An Introduction to Variational Inequalities and Their Applications*. Academic Press, New York, 1980.

[18] A. Linke. *Divergence-free mixed finite elements for the incompressible Navier-Stokes Equation*. PhD thesis, Erlangen Univ., 2008.

[19] G. Matthies and L. Tobiska. Mass conservation of finite element methods for coupled flow-transport problems. *Int. J. Comput. Sci. Math.*, 1(2-4):293–307, 2007.

[20] J. Qin. *On the convergence of some low order mixed finite elements for incompressible fluids*. PhD thesis, Penn. State Univ., 1994.

[21] O. Schenk, K. Gärtner, G. Karypis, S. Röllin, and M. Hagemann. PARDISO Solver Project. URL: http://www.pardiso-project.org, 2010. Retrieved 2010-02-15.

[22] A. Schmidt, K. Siebert, C.-J. Heine, D. Köster, and O. Kriessl. Alberta - an adaptive hierarchical finite element toolbox. URL: http://www.alberta-fem.de/, 2007. Retrieved 2010-04-28.

[23] J. Schöberl. Netgen version 4.4. URL: http://www.hpfem.jku.at/netgen/, 2008. Retrieved 2008-10-13.

[24] J. R. Shewchuk. triangle version 1.6. URL: http://www.cs.cmu.edu/˜quake/triangle.html, 2007. Retrieved 2007-09-26.

[25] H. Si. TetGen version 1.4.2. URL: http://tetgen.berlios.de/, 2007. Retrieved 2007-09-26.

[26] H. Si, K. Gärtner, and J. Fuhrmann. Boundary conforming Delaunay mesh generation. *Comput. Math. Math. Phys.*, 50:38–53, 2010.

[27] T. Streckenbach, J. Fuhrmann, H. Langmach, and M. Uhle. Pdelib- a software toolbox for numerical computations. URL: http://www.wias-berlin.de/software/pdelib/, 2009. Retrieved 2010-04-28.

[28] R. Temam. *Navier-Stokes equations*. Elsevier, North-Holland, 1991.

[29] H. Wang. *Electrocatalytic oxidation of adsorbed CO and methanol on Mo, Ru and Sn modified poly- and mono-crystalline platinum electrodes: A quantitative DEMS study (chinese)*. PhD thesis, Beijing Normal Univ., 2001.

[30] S. Zhang. A new family of stable mixed finite elements for the 3D Stokes equations. *Math. Comp.*, 74(250):543–554, 2005.